Journal of Materials Chemistry C

RSC Publishing

PAPER

View Article Online
View Journal | View Issue

Cite this: *J. Mater. Chem. C*, 2013, **1**, 5733

Enhanced phosphor conversion efficiency of GaN-based white light-emitting diodes having dichroic-filtering contacts†

Seung Jae Oh,[a] Gyeongmin Go,[a] Jong-Lam Lee,[a] E. Fred Schubert,[b] Jaehee Cho[c] and Jong Kyu Kim*[a]

Received 15th May 2013
Accepted 18th July 2013

DOI: 10.1039/c3tc30914b

www.rsc.org/MaterialsC

White light-emitting diodes (LEDs) based on the combination of a GaN-based blue LED chip and a yellow phosphor layer suffer from a low phosphor conversion efficiency (PCE) because a significant amount of the yellow fluorescence is emitted towards the blue LED chip where the fluorescence is partially absorbed. In this study, we greatly enhanced the PCE of a white LED by embedding a dichroic-filtering contact (DFC) which multi-functioned as a blue-transmitting but yellow-reflecting optical filter as well as a low-resistance ohmic contact to p-type GaN. Electrically conductive DFCs consisting of alternating layers of dense and nanoporous indium-tin-oxide were designed using a genetic algorithm optimization method, and experimentally realized by the oblique-angle deposition technique, which enables tuning of the refractive index of a *single* material. GaInN/GaN multiple quantum well LEDs with 3- and 5-layer DFCs show much enhanced PCEs, by 9.8% and 17.7%, respectively, while maintaining favorable electrical properties. In addition, the possibility of eliminating the trade-off between the color temperature and the luminous efficacy of typical warm-white LEDs by using a DFC is discussed.

Introduction

The combination of a GaInN blue light-emitting diode (LED) chip with a yellow phosphor layer is currently the most common approach to generating dichromatic white light for general illumination.[1–3] However, such phosphor-converted LEDs suffer from an unavoidable quantum deficit during the conversion of higher-energy blue photons to lower-energy yellow ones. In addition, due to the isotropic nature of fluorescence, a large fraction of the fluorescence impinging on the blue LED chip, die-attach paste, bonding wire, and reflector is absorbed, which causes a reduction in the overall phosphor conversion efficiency (PCE). It was reported that typical proximate phosphor configurations, including conformal phosphor coatings covering an LED chip[4] and uniform phosphor distributions in the reflector cup,[5] cause a considerable absorption loss in fluorescence, and hence, a reduction in the wall plug efficiency of white LEDs.[6] Several efforts have been made to reduce the fluorescence absorption loss, such as the use of scattered photon extraction (SPE) configuration,[7] the remote phosphor configuration with diffuse reflector cup,[5] the hemispherical encapsulant cup,[8] the enhanced light extraction by internal reflection (ELiXIR),[9] the ring remote phosphor structure,[10] the randomly textured phosphor structure by imprinting,[11] and the large micro-size cube phosphors.[12] Recently, a short wave pass edge filter consisting of multiple dielectric layers of TiO_2/SiO_2 on glass substrates was proposed, to recycle the backward-emitted fluorescence.[13] However, since the phosphor-coated SWPEF, deposited on a glass substrate, is remotely located, *i.e.*, at a considerable distance from the LED chip(s), its applicability to LED lamp designs is quite limited.

Incorporating a conductive dichroic-filtering contact (DFC), directly deposited on a blue LED chip through a wafer-level process and multi-functioning as a blue-transmitting but yellow-reflecting optical filter as well as a low-resistance ohmic contact, would be very beneficial in terms of design freedom, fabrication cost, and the overall PCE of white LED lamps. However, very limited materials are available for realizing such conductive DFCs: finding a combination of two conventional thin film materials that are conductive and transparent, yet have the large refractive index contrast necessary for achieving the dichroic function, is almost impossible.

In this study, we demonstrate phosphor-converted white LEDs with a conductive multilayer DFC consisting of a single

[a]*Department of Materials Science and Engineering, Pohang University of Science and Technology (POSTECH), San 31, Hyoja-dong, Pohang, 790-784, Korea. E-mail: kimjk@postech.ac.kr; Fax: +82-54-279-5837; Tel: +82-54-279-2149*

[b]*Future Chips Constellation, Electrical, Computer, and System Engineering Department, Rensselaer Polytechnic Institute (RPI), Troy, NY 12180, USA*

[c]*School of Semiconductor and Chemical Engineering, Semiconductor Physics Research Center, Chonbuk National University, Jeonju 561-756, Korea*

† Electronic supplementary information (ESI) available: Details of current–voltage characteristics of three types of contacts, optical modeling for calculation of power conversion efficiency, optimized structure of red-reflection-enhanced DFCs, and simulated warm white LED spectrums. See DOI: 10.1039/c3tc30914b

material, indium-tin-oxide (ITO). The multilayer DFCs are optimized by a genetic algorithm (GA) and incorporated directly on a blue LED wafer by using oblique-angle deposition (OAD). OAD allows one to precisely tune the nano-porosity and the refractive index of each ITO layer by adjusting the deposition angle. The white LEDs with conductive DFCs show much improved PCE, which is attributed to the enhanced reflection of yellow fluorescence by the DFC without sacrificing the transmittance of blue electroluminescence (EL) from the LED chip.

Ray-tracing simulations of fluorescence absorption loss

Ray tracing simulations were performed for a quantitative estimation of the fluorescence absorption in a GaN-based white LED described in Fig. 1(a). The 100 × 100 μm^2 blue LED chip consists of a 200 nm p-type GaN top layer, a 5-period InGaN/GaN (3/9 nm) multiple quantum well (MQW) active region, a 4 μm n-type GaN bottom layer, and a 100 μm sapphire substrate layer with a Ag reflector on the polished bottom side. The 100 × 100 μm^2 planar phosphor light source, consisting of 10 000 randomly distributed point sources emitting downward isotropic light rays with $\lambda = 552$ nm, was placed on top of the LED chip, so that all the light rays from the phosphor light source impinged onto the blue LED chip (this was done to investigate the downward-emitted light; in practical application, the phosphor emits 50% downward and 50% upward). The phosphor light rays travel inside the LED chip and are reflected, refracted, absorbed, and some of them are extracted from the LED and detected by detectors located over the 4 sidewalls and the top of the LED. No light is emitted out of the bottom surface due to the thick Ag reflector covering the sapphire substrate. It was assumed that there was 100% reflection by the Ag and no self-absorption by the phosphor light. The absorption of light by each layer constituting the blue LED chip was estimated, as shown in Fig. 1(b). The absorption of yellow fluorescence by the p-type GaN (200 nm) is negligible due to its small thickness (200 nm) and low extinction coefficient. However, light absorption by the InGaN/GaN MQW is as high as 7.4%; although it is very thin (~60 nm) this is attributed to the high extinction coefficient of the InGaN layer. The sapphire and the n-type GaN absorb significant optical power, 18.7% and 19.3% (for dual-pass, downward and upward), respectively, because these layers are thick and light rays can be trapped within the layers due to the total internal reflection. As a result of each layer's absorption, the cumulative absorption of the fluorescence emitted downward towards the LED chip can be as high as 44.8%. Note that the reflectance of the Ag reflector is assumed to be 100%; this means the absorption loss would be higher for real cases. The simulation results show that embedding a yellow-reflecting optical filter between the phosphor layer and the LED chip would be very beneficial for reducing the fluorescence loss in phosphor-converted white LEDs.

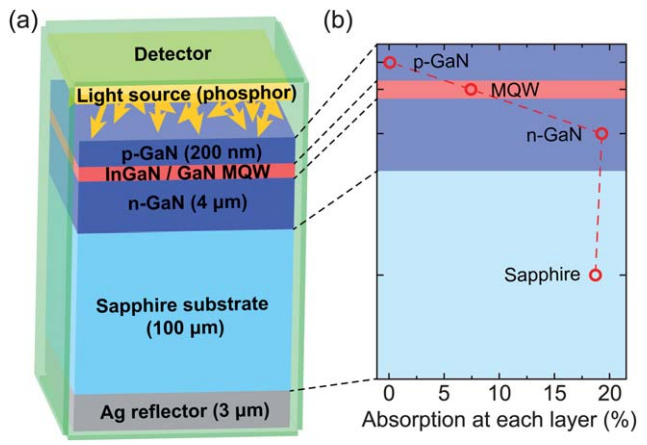

Fig. 1 (a) Schematic illustration of a GaN-based phosphor-converted dichroic white LED used for ray-tracing simulations. (b) The dual-pass absorption of yellow fluorescence by each layer constituting the LED.

Optimization of DFCs by a genetic algorithm

Fig. 2(a) shows the schematic description of a phosphor-converted white LED with a conductive DFC. The desirable functions of the DFC are (i) optical dichroic function – high transmittance for blue EL and high reflectance for yellow fluorescence, and (ii) electrical function – a low resistance ohmic contact to p-type GaN. In order to satisfy the optical and the electrical requirements simultaneously, OAD of ITO is used. ITO is chosen for its high transparency, high conductivity, and low contact resistivity to p-type GaN. The OAD method allows the fabrication of an alternating stack of high- and low-refractive index thin films made of a single material, ITO. During the OAD process, the refractive index of each ITO layer can be precisely tuned to a specific value by controlling the deposition angle, θ_{OAD}, defined as the angle between the ITO vapor flux and the substrate surface normal direction.[14–18] Fig. 2(b) shows the schematic illustration of a blue-transmitting but yellow-reflecting DFC consisting of alternating stacks of low-refractive-index nanoporous ITO and high-refractive-index dense ITO. Note that the bottom layer constituting the DFC is a dense ITO layer which forms an ohmic contact to p-type GaN.

In order to find the optimal combination of thickness and refractive index for each ITO layer, a GA method was used.[19] For the GA optimization, the figure of merit (FOM) was defined by

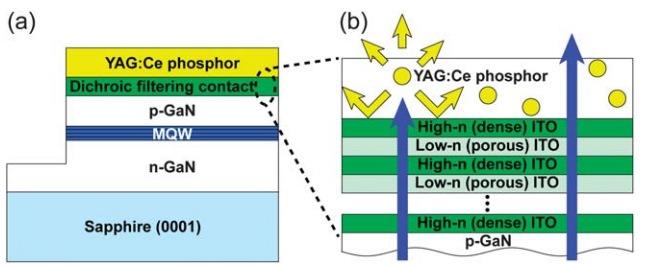

Fig. 2 (a) Schematic illustration of a phosphor-converted dichroic white LED with a DFC and (b) the structure of the DFC consisting of an alternating stack of high-refractive-index (dense) ITO and low-refractive-index (porous) ITO. The DFC functions as a blue-transmitting but yellow-reflecting optical filter as well as a low-resistance ohmic contact to the p-type GaN.

considering the EL spectrum from the blue LED and the fluorescence spectrum of YAG:Ce, as follows:

$$\mathrm{FOM} = \frac{\int_{\lambda=400\mathrm{nm}}^{\lambda=460\mathrm{nm}} w(\lambda)[1-R(\lambda)]\mathrm{d}\lambda}{\int_{\lambda=400\mathrm{nm}}^{\lambda=460\mathrm{nm}} w(\lambda)\mathrm{d}\lambda} + \frac{\int_{\lambda=460\mathrm{nm}}^{\lambda=800\mathrm{nm}} w(\lambda)R(\lambda)\mathrm{d}\lambda}{\int_{\lambda=460\mathrm{nm}}^{\lambda=800\mathrm{nm}} w(\lambda)\mathrm{d}\lambda} \quad (1)$$

where $R(\lambda)$ is the reflectance of the DFC and $w(\lambda)$ is a weighting factor based on the EL spectrum of the blue LED with $\lambda_{\mathrm{peak,blue\ LED}} \sim 430$ nm and the fluorescence spectrum of YAG:Ce with $\lambda_{\mathrm{peak,YAG:Ce}} \sim 550$ nm. Boundary conditions for the GA optimization include the highest and the lowest refractive indices measured from the dense ITO ($\theta_{\mathrm{OAD}} = 0^\circ$) and the nanoporous ITO ($\theta_{\mathrm{OAD}} = 80^\circ$) fabricated by OAD, which were 2.08 and 1.35 at $\lambda = 550$ nm, respectively. In addition, measured values of refractive indices and extinction coefficients were used in the GA optimization. Using the 30 nm dense ITO bottom layer for the formation of an ohmic contact with the p-type GaN, 3- and 5-layer DFC structures were optimized in terms of the thickness and refractive index of each layer, as summarized in Table 1.

Fig. 3(a)–(c) respectively show the calculated reflectance-contour maps of the reference ITO contact (single-layer ITO contact), the 3-layer, and the 5-layer DFCs as a function of wavelength and angle of incidence. Reflectance curves for an angle of incidence of 10° (black solid lines) and the spectrum of a typical dichroic white LED (dashed line in Fig. 3(a), used as the weighting factor $w(\lambda)$ for the GA optimization) are also shown. Note that 0° is the normal incidence of the fluorescence on the LED chip surface. Desirable optical properties of the DFC are low reflectance near $\lambda_{\mathrm{peak,blue\ LED}}$ and high reflectance near $\lambda_{\mathrm{peak,YAG:Ce}}$. However, the reflectance of the reference ITO shows ~17% near $\lambda_{\mathrm{peak,blue\ LED}}$, relatively higher than that near $\lambda_{\mathrm{peak,YAG:Ce}} \sim 7\%$. The reflectance of the 3-layer DFC has a minimum near $\lambda_{\mathrm{peak,blue\ LED}}$ and a broad high-reflection band (30–40%) at wavelengths longer than ~550 nm, indicating that the 3-layer DFC can allow more blue-transmission and more yellow-reflection than the reference ITO contact. For the 5-layer DFC, the yellow high-reflection band with a maximum value of 63% near $\lambda_{\mathrm{peak,YAG:Ce}}$ becomes narrow, maintaining the low reflection minimum near $\lambda_{\mathrm{peak,blue\ LED}}$.

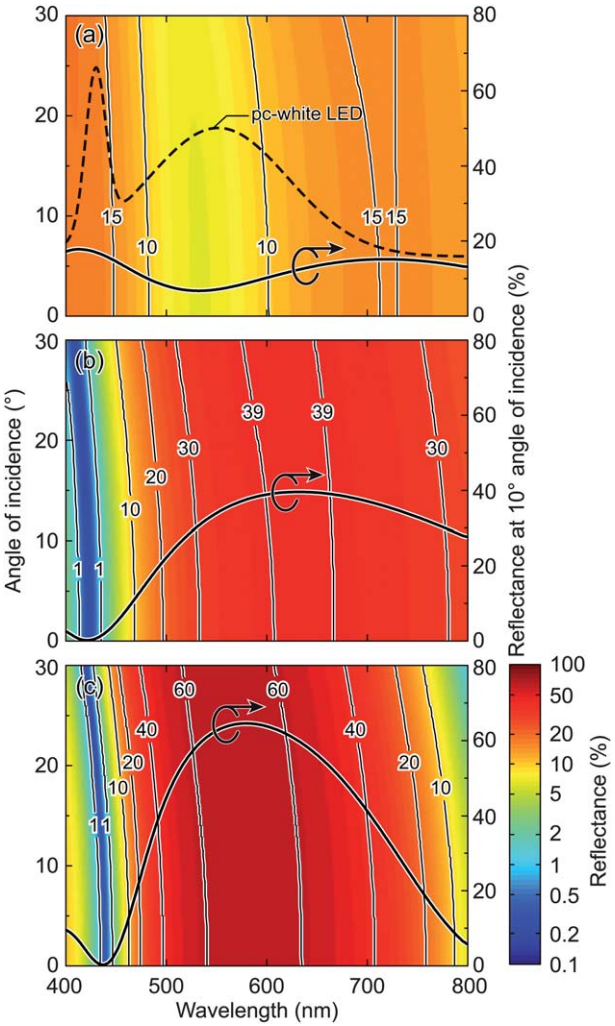

Fig. 3 Calculated optical reflectance of (a) 200 nm-thick ITO, (b) 3-layer DFC, and (c) 5-layer DFC as a function of wavelength and angle of incidence; 0° angle of incidence is the normal incidence. Reflectance curves at an angle of incidence of 10° (black solid lines) and the spectrum of a typical pc white LED (dashed line in (a)) are also shown.

Table 1 Calculated and optimized structure of a single 200 nm-thick ITO contact and multilayer DFCs on the GaN substrate and the corresponding averaged reflectance for blue (400–460 nm) and yellow (460–800 nm) wavelength regions

	200 nm ITO	3-layer DFC	5-layer DFC
Structure			Dense ITO, 79 nm Porous ITO, 114 nm
		Dense ITO, 91 nm Porous ITO, 103 nm	Dense ITO, 70 nm Porous ITO, 106 nm
	Dense ITO, 200 nm	Dense ITO, 30 nm	Dense ITO, 30 nm
R_{blue} (400–460 nm)	16.2%	2.3%	2.5%
R_{yellow} (460–800 nm)	9.3%	35.3%	59.1%
FOM	86.2	126.0	145.2

The average reflectance values in the blue and yellow spectral regions are shown in Table 1. As the number of layers increases, the yellow reflectance increases while the blue reflectance is kept low, at ~2.5%, and thus, the FOM of the DFC increases. A further increase in the number of layers results in an increase of optical absorption by the thicker ITO layers, especially at short wavelengths, reducing the blue transmittance through the DFC. Therefore 3- and 5-layer DFCs, together with the 200 nm ITO reference, were chosen for experimental demonstration.

Fabrication and characterization of DFCs

The InGaN/GaN MQW LEDs with $\lambda_{\mathrm{peak}} \sim 430$ nm were grown by metal organic chemical vapor deposition on c-plane sapphire substrates. A 2 μm- thick undoped GaN buffer layer was grown

on the sapphire substrate, followed by the growth of a 3 μm-thick Si-doped n-type GaN layer and a 5-period $In_{0.11}Ga_{0.89}N$ (3 nm)/GaN (9 nm) MQW active layer. Then, a 20 nm-thick Mg doped $Al_{0.19}Ga_{0.81}N$ electron blocking layer and a 300 nm-thick Mg-doped p-type GaN layer were grown. For LED fabrication, 350 × 350 μm^2 mesa structures were defined by standard photolithography followed by inductively coupled plasma etching. A Ti/Al/Ni/Au (30/120/40/50 nm) n-type ohmic contact was deposited by electron-beam evaporation, followed by annealing in nitrogen ambient at 650 °C for 1 min using a rapid thermal annealing system. For the reference LED, a 200 nm-thick dense ITO was deposited on the p-type GaN by electron-beam evaporation followed by a lift-off process. The 3- and 5-layer DFCs were fabricated on the p-type GaN by OAD of the ITO layer stack using electron-beam evaporation. A 30 nm-thick dense ITO layer was deposited as the ohmic contact layer to the p-type GaN, followed by the deposition of porous/dense ITO pairs. The low-refractive index porous ITO layer was formed by OAD with $\theta_{OAD} = 80°$, and then the dense ITO layer was subsequently formed on the porous ITO layer without substrate tilting ($\theta_{OAD} = 0°$). All the LEDs were annealed in oxygen ambient at 550 °C for 1 min to form ohmic contacts to the p-type GaN and to enhance their optical transparency. Finally, Ti/Au wire-bond-pad metal was deposited on both the p-type and the n-type contacts.

Experimental results and discussion

Fig. 4 shows the cross-sectional scanning-electron microscopy (SEM) images of the reference 200 nm-thick ITO, the 3-layer, and the 5-layer DFCs on p-type GaN. The refractive index profiles of each layer measured by ellipsometry are also shown. The fabricated structures show clear interfaces, well-matched layer thicknesses and refractive indices with the designed structures described in Table 1. Since the diameter of ITO nanorods and the size of the voids between them are much smaller than the wavelength of interest, light scattering by the nanoporous ITO structures is expected to be negligible.

Fig. 5(a) shows the wavelength-dependent reflectance at an angle of incidence of 10°. The overall shapes of the reflectance curves are indeed similar to the calculated ones shown in Fig. 3. As the number of layers increases, the high-reflection band becomes narrower and higher, and the peak reflectance wavelength shifts toward $\lambda_{peak,YAG:Ce}$, while the blue reflectance stays lower than that of the reference ITO contact. The average values of reflectance over 410–460 nm are 2.9% and 4.3% for the 3- and the 5-layer DFCs, respectively, which are much lower than that for the 200 nm-thick ITO reference contact, of 8.8%. On the other hand, the average values of reflectance over 460–700 nm, where yellow fluorescence dominates, are 23.3% and 29.9% for the 3- and the 5-layer DFCs, respectively, much higher than that of the reference ITO contact, of 10.6%. Despite the strong similarity in shape between the calculated (Fig. 3) and the measured (Fig. 5) reflectance curves, the measured reflectance values are lower than the calculated ones; the larger the number of layers is, the larger the deviation becomes. This discrepancy is possibly because the "dense" ITO layer deposited on top of the nanoporous ITO layer may not be as dense as the ITO on the p-type GaN, resulting in a deviation of the refractive index value from the designed one. Another possible explanation includes

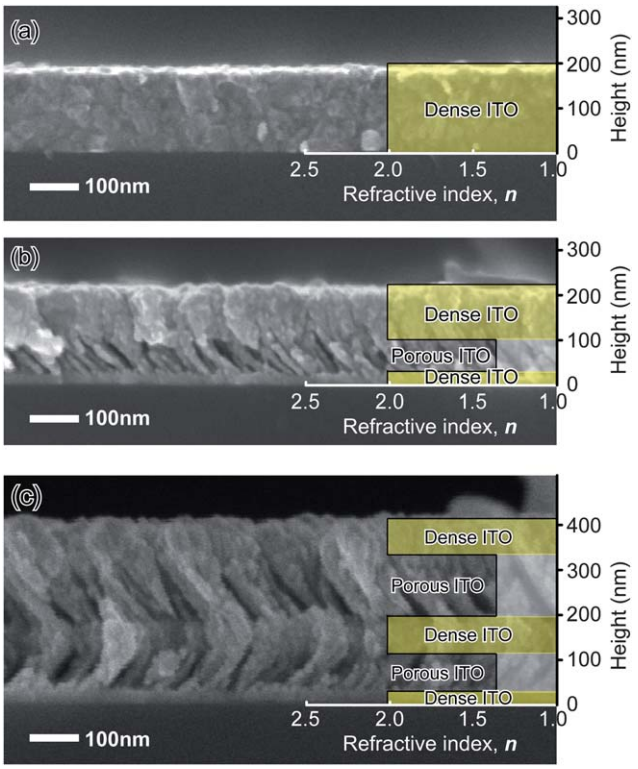

Fig. 4 Cross-section SEM images of (a) 200 nm ITO, (b) 3-layer, and (c) 5-layer DFCs made of a single material, ITO. The measured refractive indices of dense (n = 2.08) and porous (n = 1.35) ITO layers by ellipsometry are shown as a function of height from the substrate, *i.e.*, p-type GaN.

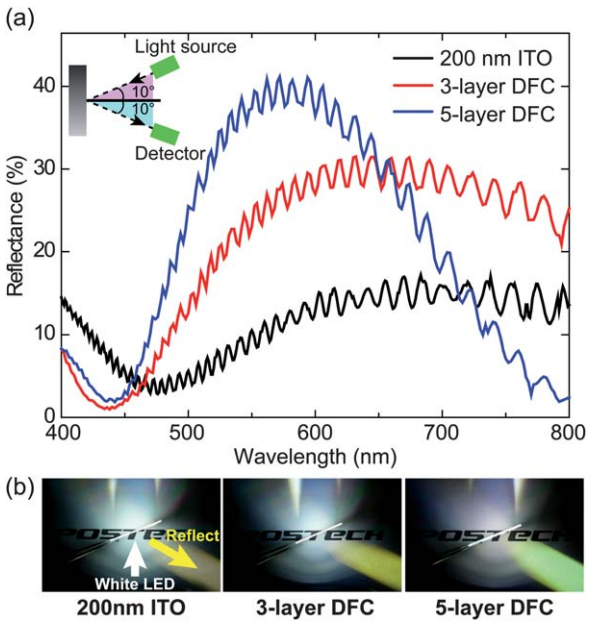

Fig. 5 (a) Measured reflectance of 200 nm-thick ITO contact, 3- and 5-layer DFCs as a function of wavelength. The angle of incidence is 10°. (b) Photographs of transmission and reflection characteristics of each sample under illumination by a dichroic white LED.

the penetration of ITO flux into the top part of the porous ITO layer, causing a different refractive index profile from the designed one. Despite such minor deviations, the optical properties of the DFCs clearly outperform those of the conventional ITO contact – much higher blue-transmission and higher yellow-reflection – which is highly promising for enhancing the overall PCE of white LEDs.

Fig. 5(b) shows photos showing the light reflected by the reference ITO contact and the DFCs fabricated on the GaN LED wafer, which are being illuminated by a dichromatic phosphor-converted white LED. The reflected light from the 200 nm-thick ITO reference contact is yellowish white (see Fig. 5(b)) originating from a weak wavelength-dependence of the reflectance, as shown in Fig. 5(a). On the other hand, the reflected light from the 3-layer and the 5-layer DFCs contain relatively more yellow and green light due to the enhanced reflectance in the yellow and green wavelength ranges.

The electrical contact properties of the reference ITO and the DFCs on GaN LEDs were estimated by using the transfer-length method (TLM). The current–voltage characteristics between the TLM pads show linear relations, *i.e.*, ohmic behaviors (Fig. S1, see ESI†). Fig. 6 shows the resistance between contact pads as a function of distance between the pads. The inset shows the optical microscopy image of 100 × 200 μm^2 TLM pads with the distance between pads of 3 μm to 15 μm with a 3 μm interval. The calculated values of the contact resistance (R_c), sheet resistance (R_{sh}), transfer length (L_T), and specific contact resistance (ρ_c) of each type of contact are summarized in Table 2. The average specific contact resistivity of the 3-layer DFC is 5.17 × 10^{-2} Ω cm^2, slightly higher than that of the reference ITO contact, 2.29 × 10^{-2} Ω cm^2. The ρ_c values for the reference ITO contact and the 3-layer DFC should be similar, since the values were obtained from the contact between the dense ITO and the p-type GaN. The difference in the ρ_c values, although it does not produce a noticeable change in the electrical properties of the LED, may stem from the change in the resistance of the DFC itself in the vertical direction; the resistance against carrier flow through a DFC increases with the increasing thickness and number of nanoporous ITO layers in the DFC. Thus, the 5-layer DFC shows an even higher ρ_c of 1.74 × 10^{-1} Ω cm^2 since it contains two nanoporous ITO layers (106 + 114 nm) and four porous/dense ITO interfaces. Note that the specific contact resistivity of ITO contacts on p-type GaN can be reduced by the deposition of a thin (<5 nm) metal (Ag[20] or Ni,[21,22] *etc.*) before the ITO deposition without a remarkable change in optical properties offered by the DFCs.

Table 2 Contact resistance (R_c), sheet resistance (R_{sh}), transfer length (L_T), and specific contact resistance (ρ_c) values of 200 nm thick ITO, 3- and 5-layer DFCs measured by the TLM method

	200 nm ITO	3-layer DFC	5-layer DFC
R_c (kΩ)	7.50	11.03	20.99
R_{sh} (kΩ)	980	941	1015
L_T (μm)	1.53	2.34	4.14
ρ_c (Ω cm^2)	2.29 × 10^{-2}	5.17 × 10^{-2}	1.74 × 10^{-1}

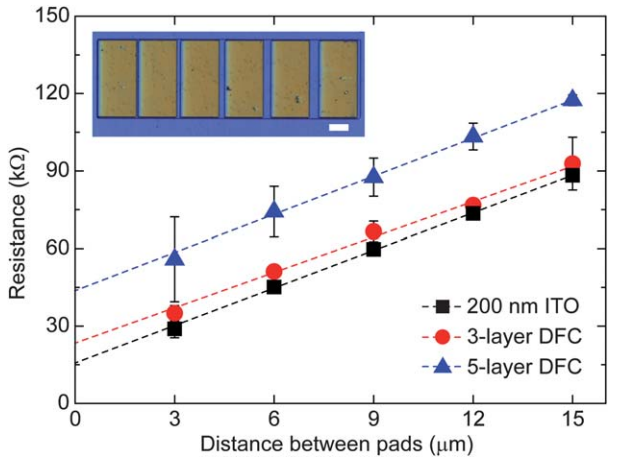

Fig. 6 Contact resistances of 3 different contacts by the TLM method. The average specific contact resistivities of 200 nm-thick ITO, 3- and 5-layer DFCs are 2.29 × 10^{-2} Ω cm^2, 5.17 × 10^{-2} Ω cm^2, and 1.74 × 10^{-1} Ω cm^2, respectively. The inset shows the rectangular TLM pattern with 3, 6, 9, 12, and 15 μm spacing between pads. Scale bar is 50 μm.

Fig. 7(a) and (b) show light output power (LOP)–current–voltage (*L–I–V*) characteristics and optical microscopy images of the blue LED chips having the reference ITO contact, the 3-layer, and the 5-layer DFCs. The LED with the 3-layer DFC shows much higher blue LOP than the reference LED due to (i) the reduced reflectance in the blue wavelength region as shown in Fig. 5(a), and (ii) less absorption in the 3-layer DFC (total thickness ~210 nm) than in the reference ITO (200 nm). The LOP of the LED with the 5-layer DFC is lower than that of the LED with the 3-layer DFC, possibly due to the increased absorption by the thicker DFC, but it is still higher than that of the reference LED owing to the reduced blue reflection. As the number of layers increases, the absorption increases and the measured optical properties deviate more from the calculated ones, possibly due to increased structural imperfections, which may degrade the electrical *I–V* characteristics as well. For the 5-layer DFC, severe current crowding, indicated by red ellipsis in Fig. 7(b), occurs near the p-type contact pad region due to the structural imperfections of the nanoporous ITO layer, and this may cause an increased contact resistance.

The enhancement in the overall PCE of white LEDs by incorporating the 3- and the 5-layer DFCs is calculated based on experimentally acquired values of blue EL, reflectance of yellow fluorescence, and simulated absorption by the blue LED chip. Fig. 8(a) shows emission spectra from a blue LED chip, and a white LED, which can be deconvoluted into a blue EL spectrum transmitted through the phosphor layer and yellow fluorescence. The LOP of each of the components can be determined by integrating the spectra over wavelength. *A*, *B*, and *C* are LOPs of the blue LED without the phosphor layer, the transmitted blue passing through the phosphor layer, and yellow fluorescence, respectively. Thus, (*A–B*) represents the optical power of the absorbed blue EL by the phosphor layer, and the overall PCE of a white LED can be expressed as

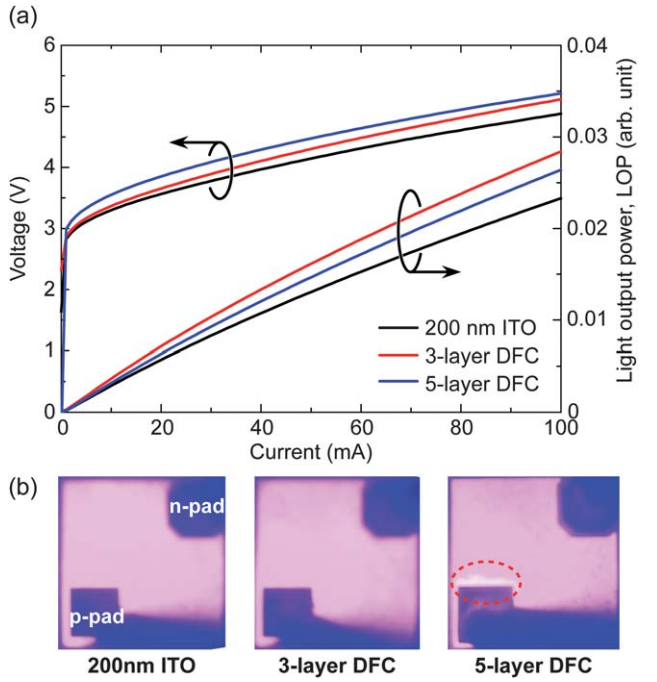

Fig. 7 (a) *L–I–V* characteristics and (b) optical microscope images of GaInN LEDs with 200 nm-thick ITO contact, 3- and 5-layer DFCs. The images were taken under the forward current of 100 mA. In the 5-layer DFC, current crowding occurred near the p-pad region (red ellipsis) due to the structural imperfection of the 5-layer DFC.

$$\mathrm{PCE} = \frac{C}{A-B} = \frac{1}{2}(1-\cos\theta_C) \times \left\{\frac{1}{2}\left(1-\frac{1}{2}\alpha\right) + \frac{1}{2}R\left(1-\frac{3}{2}\alpha\right) + \frac{1}{2}(1-R)\beta\left(1-\frac{3}{2}\alpha\right)\right\} \quad (2)$$

where θ_c is the critical angle between the phosphor layer and air, α is the self-absorption percentage of yellow fluorescence in the phosphor layer, R is the reflectance of the fluorescence by the p-contacts (the reference ITO and the DFCs), and β is the fraction of extracted yellow fluorescence impinging onto the LED chip. The first summand in the curly braces on the right-hand side of the equation is the fluorescence directed toward air (upward). The second and third summand represent the downward fluorescence reflected by the p-contact and the extracted fluorescence travelling inside the LED chip, respectively. The derivation of the above equation and associated explanations are described in ESI.†

Fig. 8(b) shows the average reflectance for blue EL and yellow fluorescence by the reference ITO contact, the 3- and the 5-layer DFCs. The average reflectance values are estimated from the measured reflectance curves shown in Fig. 5(a). The average reflectance of the DFCs in the blue wavelength region is lower than that of the reference ITO, while the average reflectance in the yellow region increases as the number of layers increases. The combination of a reduced reflectance for blue EL and an enhanced reflectance for yellow fluorescence results in a much enhanced overall PCE for the 3- and the 5-layer DFCs. The PCE

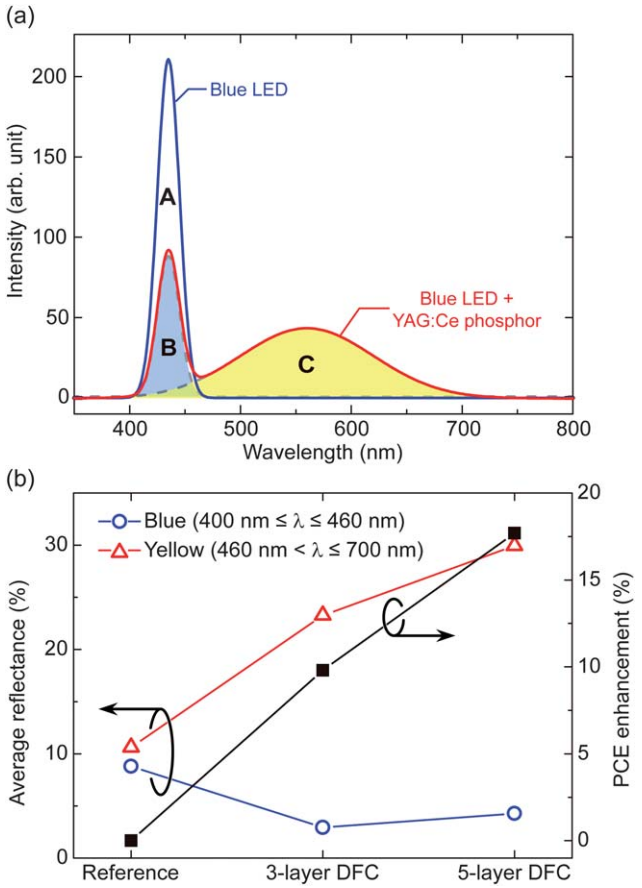

Fig. 8 (a) Schematic illustration of EL intensity from the LED through the p-contact (*A*), EL intensity passing through the phosphor layer (*B*), and yellow PL intensity (*C*). (b) Average reflectance of blue and yellow light by 200 nm-thick ITO, 3- and 5-layer DFCs over the wavelength range from 400 nm to 460 nm (blue) and from 460 nm to 800 nm (yellow). The PCE was calculated by optical modeling using the wavelength-averaged reflectance of each contact.

enhancements of LEDs with the 3- and the 5-layer DFCs, over LEDs with the 200 nm-thick ITO contact, are estimated to be as high as 9.8% and 17.7%, respectively.

Fig. 9 shows the emission spectra of white LEDs with three different contacts measured under a forward current of 100 mA, normalized with respect to the blue EL peak so that the enhancement of yellow fluorescence by the DFCs can be clearly seen. As shown in the inset of Fig. 9, a phosphor-coated glass slide (the same slide used for all three types of LEDs) is located remotely from the LEDs during the measurement. Compared to the LED with the reference ITO contact, the yellow fluorescence of LEDs with the 3- and the 5-layer DFCs is much improved due to the enhanced transmission of blue EL through the DFC and the increased reflection of the downward yellow fluorescence; without a DFC, a large portion of the yellow fluorescence will be absorbed by the LED chip. We estimate that the luminous efficacy of the LED devices incorporating the dichroic filter will be increased by more than 11%. Given the anticipated widespread use of LED lighting, an 11% enhancement in luminous efficacy would have enormous beneficial consequences. Luminous efficiency (lm W^{-1}) for the three LEDs has not been measured and compared because they have different correlated

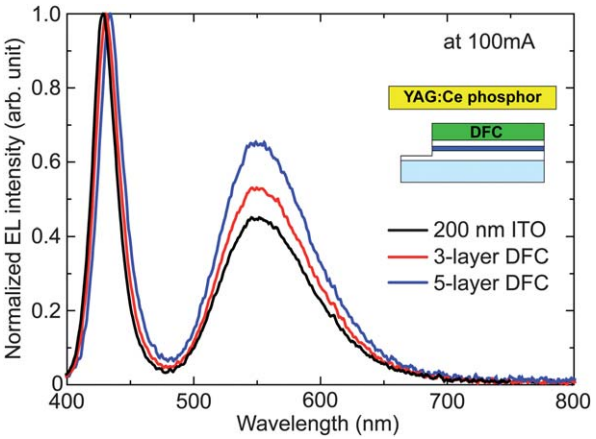

Fig. 9 Measured spectra of white LEDs with 200 nm-thick ITO contact, 3-layer, and 5-layer DFCs using the same phosphor layer for all three configurations.

color temperatures which limits the usefulness of a direct comparison of luminous efficiency. Note that the LED with the 5-layer DFC shows stronger yellow fluorescence (despite its lower blue EL) than the LED with the 3-layer DFC, due to its high reflection band, which is well-matched to the yellow fluorescence spectrum of the YAG:Ce phosphor. However, because of the increased structural imperfections of the 5-layer DFC in this study, which may cause some electrical degradation, we believe that the 3-layer DFC exhibits the best performance when taking both optical and electrical properties into consideration.

Future perspectives: towards high efficiency and high quality warm white LEDs

Despite the successful commercialization of dichromatic white LEDs based on the combination of a blue LED and a yellow phosphor layer, there is a strong demand for high "quality" white light, with a high color rendering index and low correlated color temperature (CCT). One of the ways to achieve such quality white light from LEDs is to add an extra phosphor that emits red fluorescence with a peak emission wavelength around 650 nm and large full width at half maximum when excited by 460 nm blue light[23,24] into the yellow phosphor layer. However, there are several drawbacks with regard to this trichromatic white LED (a blue LED with yellow and red phosphors) in terms of luminous efficiency: (i) the inevitable quantum deficit, *i.e.*, the large Stokes shift of red phosphors, reduces efficiency, and (ii) the inefficiency of red phosphors excitable at 460 nm. Therefore, there is a trade-off between the quality of light and the luminous efficacy of radiation. This trade-off can be mitigated or even eliminated by incorporating a DFC having blue-transmitting but red (also yellow)-reflecting characteristics.

GA-optimization calculations of red-reflection-enhanced DFCs were performed by considering the red fluorescence spectrum of a typical red phosphor emitting at 650 nm. The reflectance curves of the reference and of red-reflection-enhanced 3-, 5-, and 7-layer DFCs and resultant white LEDs' spectra are shown in supplemental Fig. S3 (see ESI†), together with the optimized DFC structures (see ESI, Table S1†).

Fig. 10(a) shows the chromaticity coordinates of simulated emission spectra from trichromatic white LEDs, indicated by open squares on the Commission International d'Eclairage (CIE) 1931 diagram. As a result of the enhanced emission of the yellow and red fluorescence by the red-reflection-enhanced DFCs (see ESI, Fig. S3†), the chromaticity coordinate moves from lower left to upper right along the Planckian locus as the number of layers in the DFC increases. This indicates that the CCT decreases from 4309 K (reference LED) down to 3957 K (LED with a 7-layer DFC) as a result of the enhanced extraction of fluorescence by the DFCs, especially in the red wavelength region, as shown in Fig. 10(b). Furthermore, the combined effect of the enhanced EL from the blue LED and the enhanced red and yellow fluorescence by the DFCs results in an increase in the

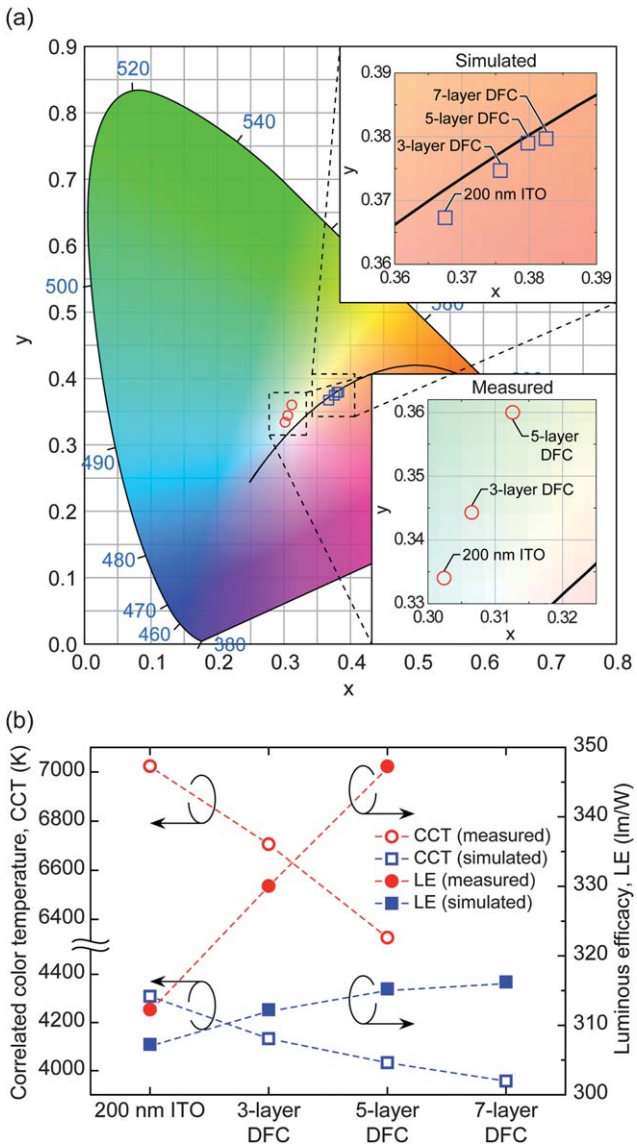

Fig. 10 (a) The chromaticity coordinates of simulated emission spectra from trichromatic white LEDs with 200 nm ITO, 3-, 5-, and 7-layer DFCs (open squares) and measured EL spectra (Fig. 9) from dichromatic white LEDs with 200 nm ITO, 3-, and 5-layer DFCs (open circles) on the CIE 1931 diagram, respectively. (b) The correlated color temperature and the luminous efficacy of trichromatic and dichromatic white LEDs calculated from the simulated and measured emission spectra, respectively.

luminous efficacy of radiation, together with a decrease in CCT with the increasing number of layers (Fig. 10(b)). Open circles in Fig. 10(a) indicate the chromaticity coordinates of experimentally measured EL spectra from the dichromatic white LEDs shown in Fig. 9. Since the spectrum of dichromatic LEDs is different from that of trichromatic LEDs, the values of CCT and luminous efficacy are also different. However, the overall tendency of change in the chromaticity coordinates is similar to that of the simulated trichromatic white LED: the CCT decreases from 7022 K (reference LED) down to 6326 K (LED with a 5-layer DFC), whereas the luminous efficacy of radiation increases from 312 to 347 lm W^{-1}, owing to the enhanced extraction of both EL from the LED and the fluorescence in the yellow wavelength region by the DFCs. This strongly suggests that it is possible to reduce or eliminate the present trade-off between the CCT and the luminous efficacy of radiation of white LEDs, by using properly designed DFCs that enhance the yellow and the red fluorescence as well as the blue EL.

Conclusions

In summary, we have demonstrated the enhancement of the PCE of dichroic white LEDs by incorporating DFCs to serve as optical filters with high blue-transmittance and high yellow-reflectance and as low-resistance ohmic contacts. The GA optimized DFCs, which consist of alternating stacks of dense and nanoporous ITO layers fabricated by OAD, reduce the blue reflection and enhance the yellow reflection. As a result, the blue EL from GaN-based LED chips coated with a 3- and a 5-layer DFC was much enhanced, while exhibiting a specific contact resistivity comparable to that of a reference 200 nm-thick ITO contact. The enhancement of the overall PCE values of the LEDs with a 3- and a 5-layer DFC is estimated to be 9.8% and 17.7%, respectively, mainly due to the enhanced reflection of yellow fluorescence. Furthermore, the limiting trade-off between the CCT and the luminous efficacy of radiation of typical warm-white LEDs can be overcome by an optimized DFC, which paves the way to realize warmer yet more efficient white LEDs.

Acknowledgements

The authors gratefully acknowledge support from the International Collaborative R&D Program funded by MKE and KIAT, the IT R&D Program of MKE/KEIT (10035598), and the Industrial Strategic Technology Development Program (10041878) funded by MKE, and the Basic Science Research program through the National Research Foundation of Korea (NRF) funded by the Ministry of Education, Science and Technology of Korea (2010-0006646).

Notes and references

1 K. Bando, Y. Noguchi, K. Sakano and Y. Shimizu, *Tech. Digest, Phosphor Res. Soc. 264th meeting, 5-14*, November 29, 1996.
2 S. Nakamura and G. Fasol, *The blue laser diode: GaN based light emitters and lasers*, Springer, Berlin, 1997.
3 R. Mueller-Mach, G. O. Mueller, M. R. Krames and T. Trottier, *IEEE J. Sel. Top. Quantum Electron.*, 2002, **8**, 339–345.
4 D. A. Steigerwald, J. C. Bhat, D. Collins, R. M. Fletcher, M. O. Holcomb, M. J. Ludowise, P. S. Martin and S. L. Rudaz, *IEEE J. Sel. Top. Quantum Electron.*, 2002, **8**, 310–320.
5 J. K. Kim, H. Luo, E. F. Schubert, J. Cho, C. Sone and Y. Park, *Jpn. J. Appl. Phys.*, 2005, **44**, L649–L651.
6 J. P. Kim, *International LED and Green Lighting Seminar 2012*, Kintex, Korea, 2012.
7 N. Narendran, Y. Gu, J. P. Freyssinier-Nova and Y. Zhu, *Phys. Status Solidi A*, 2005, **202**(6), R60–R62.
8 H. Luo, J. K. Kim, E. F. Schubert, J. Cho, C. Sone and Y. Park, *Appl. Phys. Lett.*, 2005, **86**, 243505.
9 S. C. Allen and A. J. Steckl, *Appl. Phys. Lett.*, 2008, **92**, 143309.
10 M. T. Lin, S. P. Ying, M. Y. Lin, K. Y. Tai, S. C. Tai, C. H. Liu, J. C. Chen and C. C. Sun, *IEEE Photonics Technol. Lett.*, 2010, **22**, 574–576.
11 H. C. Chen, K. J. Chen, C. H. Wang, C. C. Lin, C. C. Yeh, H. H. Tsai, M. H. Shih, H. C. Kuo and T. C. Lu, *Nanoscale Res. Lett.*, 2012, **7**(1), 188–192.
12 H. K. Park, J. H. Oh and Y. R. Do, *Opt. Express*, 2012, **20**, 10218–10228.
13 J. R. Oh, S. H. Cho, Y. H. Lee and Y. R. Do, *Opt. Express*, 2009, **17**, 7450–7457.
14 J. Q. Xi, M. F. Schubert, J. K. Kim, E. F. Schubert, M. Chen, S. Y. Lin, W. Liu and J. A. Smart, *Nat. Photonics*, 2007, **1**, 176–179.
15 J. K. Kim, S. Chhajed, M. F. Schubert, E. F. Schubert, A. J. Fischer, M. H. Crawford, J. Cho, H. Kim and C. Sone, *Adv. Mater.*, 2008, **20**, 801–804.
16 M. F. Schubert, J. Q. Xi, J. K. Kim and E. F. Schubert, *Appl. Phys. Lett.*, 2007, **90**, 141115.
17 X. Yan, F. W. Mont, D. J. Poxson, J. Cho, E. F. Schubert, M. H. Kim and C. Sone, *J. Appl. Phys.*, 2011, **109**, 104113.
18 D. J. Poxson, F. W. Mont, M. F. Schubert, J. K. Kim and E. F. Schubert, *Appl. Phys. Lett.*, 2008, **93**, 101914.
19 D. J. Poxson, F. W. Mont, M. F. Schubert, J. K. Kim, J. Cho and E. F. Schubert, *Opt. Express*, 2010, **18**, A594–A599.
20 J. O. Song, D. S. Leem, J. S. Kwak, Y. Park, S. W. Chae and T. Y. Seong, *IEEE Photonics Technol. Lett.*, 2005, **17**, 291–293.
21 R. H. Horng, D. S. Wuu, Y. C. Lien and W. H. Lan, *Appl. Phys. Lett.*, 2001, **79**, 2925–2927.
22 Y. C. Lin, S. J. Chang, T. Y. Tsai, C. S. Chang, S. C. Shei, S. J. Hsu, C. H. Liu, U. H. Liaw, S. C. Chen and B. R. Huang, *IEEE Photonics Technol. Lett.*, 2002, **14**, 1668–1670.
23 E. F. Schubert, *Light-Emitting Diodes*, Cambridge University Press, Cambridge, 2007.
24 Y. Narukawa, *Opt. Photonics News*, 2004, **15**, 24–29.

